Correlation of wear and work in dual pivoted jaw crusher tests

J.Terva[1*], K.Valtonen[1], P. Siitonen[2], V.-T. Kuokkala[1]

[1]*Tampere Wear Center, Department of Materials Science, Tampere University of Technology, P.O. Box 589, FI-33101 Tampere, Finland.*
[2]*Metso Minerals Inc., P.O. Box 306, FI-33101 Tampere, Finland.*

Abstract

A laboratory sized jaw crusher with uniform movement of the jaws, the Dual Pivoted Jaw Crusher (DPJC), was used to determine the relationship between wear and work. Wear was concentrated on the jaw plates opposing each other and was measured as mass loss of the specimens. Work was measured directly from the force and the displacement of the instrumented jaw, which allowed work to accumulate only from the actual crushing events. The tests were conducted with several jaw geometries and with two motional setups, where the relation of compressive and sliding motion between the jaws was varied.

The comminution of rock is presumed to be irreversible, meaning that the energy used for crack formation in the rock particles eventually results in the fracture of the particles. Therefore, the amount of energy needed to comminute rock particles should be roughly constant and not dependent on the loading conditions, if the speed of the loading contact is not changed. The DPJC test method allows the separation of work components into comminution specific work and sliding specific work. The results can be used to compare the crushability of minerals without the influence of the used test geometry or the selected jaw plate materials. The sliding work can be used for the comparison of the wear of the jaw plate materials.

Keywords: Jaw crusher, Comminution, Work, Crushability, Abrasive wear.

*Corresponding author: Juuso Terva (juuso.terva@tut.fi).

1. INTRODUCTION

Modern society requires vast amounts of resources in order to function properly. For example, the production of goods requires energy and raw materials, which both can be obtained from the Earth's crust. The excavation of the resources also consumes plenty of energy, the amount of which spent for example on comminution and grinding is globally nearly 2% of all generated energy [1]. Quarrying involves several steps to produce the required products: blasting, crushing (primary, secondary), and grinding (coarse, fine). In addition, transportation of boulders, stones, or sand is needed between the steps. The above mentioned steps require different amounts of energy depending on the size reduction method and the choice of the equipment. The reduction ratio (RR) of each step is the ratio between the size of the feed and the product of the crushing equipment. Explosive blasting and crushing of boulders is considered to be the most efficient method of size reduction [2]. Each following reduction step has a decreasing crushing efficiency, where increasing amounts of work are needed in order to reduce the rock size by the same ratio than in the previous step [2].

The efficiency of size reduction is generally very low, and the estimated amount of energy actually used for splitting particles and generation of new surfaces can be around 1% to 3% from the total amount of energy put into the system [3,4]. Some of the energy is lost in the operation of the equipment as friction, vibrations, electrical loss, and heat. A jaw crusher running empty is reported to consume half of the amount of energy compared to the jaw crusher operating at the maximum capacity [5]. The crusher stores energy also elastically when the rock particles are compressed, and can lose this energy as vibrations when the compression is suddenly released due to fracturing. The application of a sufficient compressive stress increases the tensile stresses around the defects until at a critical stress level the compressed particle fractures. The amount of elastic energy stored in the particle is lost due to the spring-back motion, which causes movement of the fractured particles and eventually transfers to heat. If the critical stress for particle fracture is not reached, the elastic work can return to the system with some (small) part of it possibly being

used to increase the size and amount of the defects in the mineral. The increased size and density of the defects can lower the critical stress required for fracturing in the next compressive cycles. For example, the amount of defects caused by explosive blasting has been found to affect the energy consumption of the following reduction step [6, 7]. Schoenert [8] showed with quartz glass that particle fracture can also occur during the unloading phase, as the stress fields introduced during the compression phase can remain after unloading and result in particle breakage. The size distribution of the product was much coarser when the particle fracture occurred in the unloading phase compared to the product produced during the loading phase.

Some energy is consumed in the contacts between the rock particles and the surfaces used to apply the compressive forces. The material commonly used in jaw and cone crushers is austenitic manganese steel due to its good ability to work harden. In addition to compression, the crushing contact between a metal and a mineral can have a sliding component, which causes friction and energy losses as heat. The compressional and sliding movement can also deform the steel surface plastically, which again requires energy. The movement of the rock particles on the metallic surfaces causes abrasive wear, which can also be seen as an indirect loss of energy as the cost of manufacturing of a new wear part.

This paper concentrates on the wear and work relation during comminution of rock, studied with a small laboratory size jaw crusher called the dual pivoted jaw crusher. The studied feed size of 10 mm–12.5 mm is in the coarse grinding range of the reduction steps, as defined by Hukki [2]. The small size of the feed for a jaw crusher can cause variations in the energy consumption per reduction step, which needs to be taken into account when comparing the results with the energy consumption of larger equipment. In general, determination of the correlation of wear and work is difficult in the tests where the amount of frictional work due to sliding is high compared to the amount of wear produced. Avient et al. [9] showed abrasive wear to be proportional to the normal force and the coefficient of friction, when the scratched test materials were metallic. Goddard [10], however, found no linearity between wear and friction when using the same test configuration for non-metallic materials because of fracturing of the materials on the sides of the grooves.

The motivation of this study is to better understand the crushing environment and how the various factors are interconnected. A common single-toggle jaw crusher design consists of a jaw plate that is fixed to the frame, and of a moving jaw plate that is moved by rotating an eccentric axle. A flywheel, which is connected to the axle, is used to store kinetic energy supplied by an electric motor. The momentum of the flywheel keeps the crushing motion of the jaw fairly constant, which is only slightly reduced by the crushing events. The jaw crusher is usually choke fed, meaning that the gape between the jaws has multiple rock particles at the same time. If the gape is filled too full, the momentum stored in the flywheel decreases, which may cause a seizure. Therefore the capacity, or the flow of the particles through the gape of the jaw crusher, has a certain maximum value. The crushing capacity is affected by various parameters, for example by the opening angle of the jaws, the movement pattern of the jaws, the throw and the open and closed site settings, the material and profile of the jaw plates, and the mechanical and tribological properties of the crushed rock. The movement pattern of the moving jaw in the single toggle jaw crusher is elliptical at the release end of the jaw and circular at the feed end. The extent of movement also increases towards the feed end. This means that the movement pattern is different along the jaw and that the direction of movement is different in different ends of the gape: the release end of the single-toggle jaw crusher closes at the same time the feed end opens, and vice versa. This effect causes smaller rocks to become crushed while larger rocks fall lower in the gape, and larger rocks to become crushed while smaller rocks fall lower or out of the gape.

Gouging abrasion wear tests according to the ASTM G81-97 [11] standard are generally conducted with a laboratory sized version of the above mentioned single-toggle jaw crusher. Korman et al. [12] measured the work done by the jaw crusher from the electrical power taken by the motor. This approach is quite good for overall measurement of the energy consumption, but it cannot be used to investigate the crushing situation further. Implementation of force sensors for the measurement of the contact loads during crushing is also hindered by the unknown location of the crushing events. Also the movement pattern of the jaw at the point of crushing is unknown, as it varies along the jaw length. However, several types load cells have been used to determine the force levels, coefficient of friction, and pressure distribution in the tests with a common single-toggle jaw crusher [13].

The dual pivoted jaw crusher was designed to study the effects of crushing with a certain movement pattern, which is the same at every level. This allows measurement of the contact forces during the movement of the

jaws, which can then be used to calculate the energy consumed in the crushing events. In other words, this method does not measure the work done by the motor powering the equipment, but it measures only the actual work of the crushing events. With the power measurement method of the common single-toggle jaw crusher, the work needed to run an empty crusher can of course be subtracted from the total power consumption of the crusher, but it is not certain whether the empty and fully loaded jaw crushers would have the same energy consumption after the actual work of rock crushing is subtracted.

2. TEST METHOD

The dual pivoted jaw crusher DPJC was used to conduct tests with several different setups. Figure 1a and b show the DPJC equipment, and Figure 1c is a functional schematic of the DPJC. Both jaw frames are connected to the upper and lower pivot points, which are highlighted in the images as black lines and circles. Jaw1 frame is on the left hand side and Jaw2 on the right hand side of the crushing cavity, and both frames are identical. The distance D between the pivot points of the left and right jaw frames is set to a constant 60 mm at both ends, which causes the jaw frames to remain parallel when the frames are rotated around the upper pivot points. The upper pivot points are axles supported by a cylindrical body fixed to the back plate. The cylindrical body can be rotated, which again rotates the angle β of the line between the pivot points from the horizontal level. The lower pivot points are axles supported by a disc. The disc can be rotated inside two flanges that can be tightened to set the angle β between the vertical level and the line between the pivot points. The flanges are connected to two linear bearings allowing movement only in the Z and Y directions and preventing rotations. A flywheel, which is rotated by an electric motor, is connected to the flanges with a shaft. The shaft length and connection point to the flywheel can be changed, which causes different extent of rocking motion in the jaw frame, when the flywheel is rotated. The angle α describes how much the jaw frame setup is rotated from the vertical level. The change of angle β causes a different movement pattern of the frame, when the rocking motion is the same. Figure 1b shows another setup, where the β angle is set to 0°. At β = 0°, the rocking motion causes movement mainly perpendicularly to the long side of the jaw frames, which in effect causes compressive movement in the Z direction between the jaw frames. At β = 90°, as shown in Figure **1**a, the movement at start is mostly in the Y direction with only minor Z movement. As α is increased, the increasing Z component begins the compressive movement. In effect the β angle changes the relation between the sliding movement in the Y direction and the compressive movement in the Z direction.

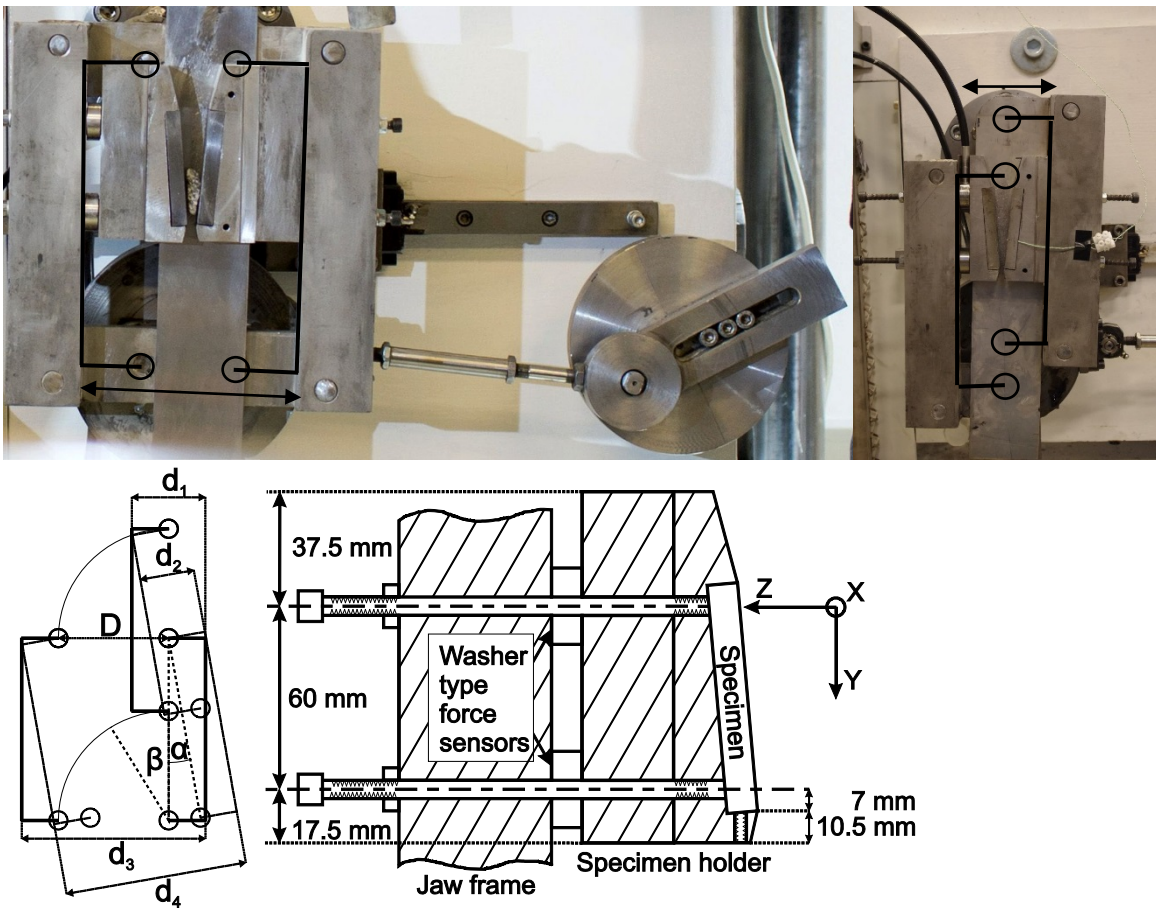

Figure 1: *Dual pivoted jaw crusher shown a) in β=90° setup, b) in β=0° setup, c) the geometrical movement between the jaw frames, and d) the assembly of the specimen holder, the force sensors, and the jaw frame.*

The jaw frame contains several through-holes that are used to tighten the specimen holder to the jaw frame with two long screws. The screws are threaded into the specimen holder and tightened on the opposite side of the jaw frame with nuts, as schematically shown in Figure **1**d. The same screws are also used to secure the washer-type force sensors into place between the specimen holder and the jaw frame. The specimen holder assembly is modular and consists of rectangular blocks for setting the correct position of the actual specimen holder, and of specimen holders for setting the angle of the specimen plate. The tests were conducted with three different jaw angles in both jaws, denoted as Jaw1 and Jaw2, as follows: 5° + 5°, 10° + 0°, and 12.5° + 12.5°. The total jaw angle is the sum of tilt angles of Jaw1 and Jaw2.

The specimens were rectangular plates with the dimensions of 75 mm x 25 mm x 10 mm. The length of the specimens was decreased to 50 mm in the tests with 12.5° + 12.5° jaw angles and β = 0°, as the gap between the jaw frames was too small to fit normal sized specimen plates at such angles. The dimension change did not affect the amount of wear or work (energy consumption) in the test, as the large opening angle prevented crushing events at the higher positions of the gape.

Figure 2 shows the movement of Jaw1 relative to Jaw2, when β = 90°. The approach of Jaw1 follows a circular path with a radius of 60 mm, which is the set distance between the pivot points of the jaw frames. In this example the Jaw2 specimen can be considered stationary and only the Jaw1 specimen is moving, as in the traditional jaw crusher design. Figures 2a and b show a comparison of the movements of specimens in Jaw1 and Jaw2 at the specimen angles of 10° + 0° and 5° + 5°, respectively. The values of the jaw angles are doubled in the picture to better illustrate the changes. F_Y and F_Z are the directions in which the force sensor measures the forces. The horizontal and vertical displacements ΔZ and ΔY are different in Figures 2a and b, even if the open and closed side settings of the setups are the same. The reason for the difference is the angle of the Jaw2 specimen. At the beginning of the approach, Jaw1 in Figure 2b is mainly vertical and the jaws are actually separating for a short moment. When the tangent of the circular path reaches the angle of the Jaw2 specimen, the actual approach begins. Figure 2c shows this effect, when the coordinate system in

Figure 2b is rotated so that Jaw2 becomes vertical. ΔZ_2 and ΔY_2 represent now the approach in the normal and perpendicular directions to the Jaw2 specimen surface. The approach is nearly the same in Figure 2a and c after Jaw1 has passed the point in c, where the tangent along the circle is vertical and the horizontal displacements ΔZ and ΔZ_2 are about the same. A noticeable difference between the setups is the relative speed in the Y direction at the point where the jaws begin to approach. The rotating flywheel causes a sinusoidal speed variation in the crushing cycle, where the speed is lowest at the beginning and the end of the approach half of the cycle and largest at the middle of the cycle. The angled Jaw2 specimen in Figure 2b delays the start of the actual approach and causes a higher relative speed between the specimen surfaces than in Figure 2b, when the jaws begin to compress the rock particles. In Figure 2a, the relative speed in the lateral direction is highest at the half point of the crushing cycle. Another factor affecting the jaw speed was that as the rotational speed of the flywheel was kept constant, the relative jaw speeds were higher with angled Jaw2 specimens, as the ΔZ and ΔY displacements in the same cycle time were larger than with the vertically angled Jaw2 setup. To conclude, even with the same total jaw angle setups of 10° + 0° and 5° + 5°, the tests have different approach and relative speeds between the Jaw1 and Jaw2 specimens.

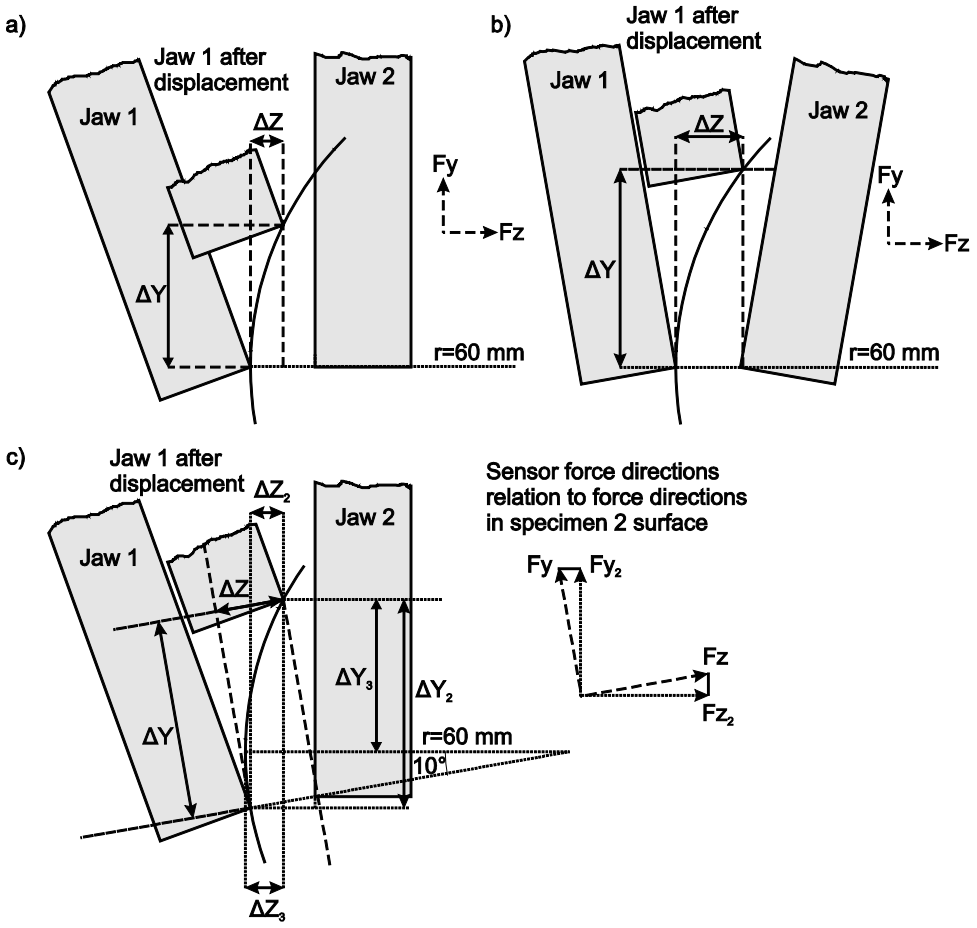

Figure 2**:** *The relative movement of the specimens in each jaw, a) when only the specimen in Jaw1 is tilted, b) both specimens are tilted by the same amount, c) the relative movement of the tilted specimens as in b) when the coordinate system is aligned with Jaw2 and the specimens are tilted similarly as in a).*

2.1 Test materials

The aggregate used in the tests was granite from Sorila, Finland. Several feed sizes of the granite were used in the tests, the largest size being10–12.5 mm. The Sorila granite contains mostly plagioclase and quartz with an average grain size of 0.7 mm. Table 1 lists the mineral content and other typical nominal properties of the Sorila granite. The Sorila granite has good uniaxial compression strength (UCS) and it is considered to be abrasive and hard to crush [14].

The test plates were made of Metso Minerals XT710 grade steel, which has a high carbon and manganese content, as seen in Table 1. The austenitic microstructure of the steel is ductile and has a good ability to work harden. The deformation mechanisms of the XT710 steel are mainly slipping and twinning, which together can result in an increase of surface hardness down to several millimeters from the wear surface in real crushing applications. XT710 steel test specimens were water jet cut from a side plate manufactured for a commercial jaw crusher. The surface receiving contacts with the rock was ground flat with a P120 grit silicon carbide paper to remove the deformed layer after the cutting process.

Table 1: *Chemical and mineral compositions of the XT710 and the Sorila granite [14].*

Element (Mass fraction %)	**XT710**	**Mineral (Mass fraction %)**	**Sorila granite**
C	1.24	Plagioclase	45
Si	0.57	Quartz	25
Mn	16.4	Feldspar	15
P	0.042	Biotite	10
S	0.005	Hornblende	5
Cr	2.44		
Ni	0.26	**Other properties**	
V	0.00	Average grain size (mm)	0.7
Mo	0.04	UCS (MPa)	193.9
Other properties		Bond w_i	16.0
Hardness (HV)	240	L.A. index	17.2
Density (g/cm^3)	7.77	Density (g/cm^3)	2.62

2.2 Test matrix

A 4 kg batch of granite was crushed in each test. Table 2 shows the other parameters used in the tests, which were named according to two different setups, S and C. Setups S describe the used β and specimen angles, and therefore contain the parameters that affect mainly the wear and energy outcomes of the test. Setup S indicates also the running number of the specimen pair used in the test. Each specimen pair was used to conduct four tests with setups C, which describe the parameters affecting the crushing and the size reduction of the rock, i.e., the minimum and maximum gaps at the release end of the jaw and the feed size. The throw, i.e., the compressive displacement of the jaw crusher, was 3 mm in all tests, whereas the lateral displacement of the jaw was changed by the parameters of setup S. Tests with setup C1 crushed 10–12.5 mm feed to product size P with min- max gap of 3.15–6 mm. Setup C2 was a continuation test, where the product P of test with setup C1 was crushed even smaller with min–max gap of 0–3 mm. The approximate reduction ratio is 2:1 for both setups C1 and C2. Tests with setup C3 crush the larger sized rock straight to the smaller size with the reduction ratio of 4:1. The use of setup C3 should lead to wear and energy consumption that are comparable to the sum of the tests with setups C1 and C2. Setup C4 is close to setup C2, as the size of the rock particles in product P was mostly 4–6.3 mm. The main differences are that C4 has a much narrower size distribution, and because of that the wear caused by 4–6.3 mm was localized to a smaller region on the specimen surfaces.

Table 2: *Test parameters used in the tests with the XT710 manganese steel specimens. One specimen pair was used to conduct all tests consecutively with the C1-C4 setups.*

Test	**Specimen pair**	**Specimen pair setup S**		**Crushing setup C**	
		β angle	specimen angles	min-max gap (mm)	rock size (mm)
S1-C1	S1	0°	5° + 5°	3.15–6	10–12.5
S1-C2	S1	0°	5° + 5°	0–3	product of C1
S1-C3	S1	0°	5° + 5°	0–3	10–12.5
S1-C4	S1	0°	5° + 5°	0–3	4–6.3
S2-C1	S2	0°	10° + 0°	3.15–6	10–12.5
S2-C2	S2	0°	10° + 0°	0–3	product of C1
S2-C3	S2	0°	10° + 0°	0–3	10–12.5
S2-C4	S2	0°	10° + 0°	0–3	4–6.3
S3-C1	S3	0°	12.5° + 12.5 °	3.15–6	10–12.5
S3-C2	S3	0°	12.5° + 12.5 °	0–3	product of C1
S3-C3	S3	0°	12.5° + 12.5 °	0–3	10–12.5
S3-C4	S3	0°	12.5° + 12.5 °	0–3	4–6.3
S4-C1	S4	90°	5° + 5°	3.15–6	10–12.5
S4-C2	S4	90°	5° + 5°	0–3	product of C1
S4-C3	S4	90°	5° + 5°	0–3	10–12.5
S4-C4	S4	90°	5° + 5°	0–3	4–6.3
S5-C1	S5	90°	10° + 0°	3.15–6	10–12.5
S5-C2	S5	90°	10° + 0°	0–3	product of C1
S5-C3	S5	90°	10° + 0°	0–3	10–12.5
S5-C4	S5	90°	10° + 0°	0–3	4–6.3
S6-C1	S6	90°	12.5° + 12.5 °	3.15–6	10–12.5
S6-C2	S6	90°	12.5° + 12.5 °	0–3	product of C1
S6-C3	S6	90°	12.5° + 12.5 °	0–3	10–12.5
S6-C4	S6	90°	12.5° + 12.5 °	0–3	4–6.3

2.3 Test analysis and equipment

Each specimen plate pair went through a running-in by crushing 4 kg of granite before the actual tests. The running-in was used to reach the steady state region of the wear rate. The wear results were obtained from the mass loss of the specimens after each test by weighing with a Precisa XT 1220M scale having a 0.001 g measurement accuracy. The volumetric wear rate per kilogram of crushed rock (g/kg) was obtained using the measured density of the XT710 steel.

The wear surfaces of the specimens were examined with Leica MZ75 stereo microscope, Leica DM2500M materials analysis microscope, and Zeiss ULTRAplus ultra high resolution field emission scanning electron microscope (FESEM). The Vickers hardness of the XT710 steel was measured with Struers Duramin A-300 hardness tester using 1 kg and 5 kg loads. The comminution product was sieved with Retsch analytical sieve shaker A-200 with sieve sizes of 10 mm, 8 mm, 6.3 mm, 4 mm, 2 mm, 1 mm, 500 µm, and 250 µm.

3. RESULTS

The dual pivoted jaw crusher tests have three main measurable outcomes: size reduction of the rock particles, wear of the specimen plates, and amount of energy consumed (or work done) in the process, which are all affected by the selected test parameters. The most important parameter leading to differences in the results of individual tests is the amount of lateral movement between the jaws.

3.1 Size of comminution product

The size of the product and the reduction ratio are mainly affected by the minimum and maximum gaps of the jaws and the feed size. Figure 3 shows the sieved size distributions of the product from tests with 5°+5° jaw angles as the fraction of material passing the sieve. Both β = 0° and β = 90° setups show similar product size distributions with similar crushing setups C. The major difference in the product size distribution is caused by the different crushing setups, the C1 setup producing the coarsest product sizes and C2 and C3 setups the finest product sizes. The C4 setup with smaller initial gravel size leads to a coarser product size than the C2 and C3 setups with the same min–max gap setting. This could be caused by the more homogeneous size of the feed being crushed near the lower end of the jaw. Moreover, the C4 product may have escaped the jaws more easily, because it has been crushed lower in the gape than the larger particles of the other feeds.

Similar relative order and about the same kind of size distribution as with 5°+5° jaw angles were obtained from the tests with 10°+0° and 12.5°+12.5° specimen angles, as shown in Figure 4 and **Figure 5**. However, there is a difference in the order when comparing the comminution with the β = 0° and β = 90° setups. The jaw angles of 5°+5° and 12.5°+12.5° lead to finer sized product in the tests with the β = 0° setup than with the β = 90° setup, while the opposite happens when the jaw angles are changed to 10°+0°. This difference in the comminution could be caused by the slight opening of the gape at the beginning of the compression cycle when the Jaw2 specimen is tilted. This opening movement (ΔZ) is shown in Figure 2c, and it may result in a larger size distribution when compared to the tests with the β = 0° setup. Figure 2a shows that there is no opening movement with the 10°+0° specimen angles.

Accordingly, the results show that the comminution of granite is mainly affected by the crushing setup C. The P_{80} value is the size of the product that is larger than 80% of the product size distribution, and is between 3 mm–4 mm for the tests with the C2 and C3 setups and between 6 mm–7 mm for the tests with the C1 setup. The corresponding F_{80} value of the 10 mm–12.5 mm feed is approximately 12 mm. The $RR=F_{80}/P_{80}$ reduction ratios for setups C1 and C3 are close to (2:1) and (4:1), respectively. In the C2 test, the product of the C1 tests was used as feed, which yields the reduction ratio of (2:1).

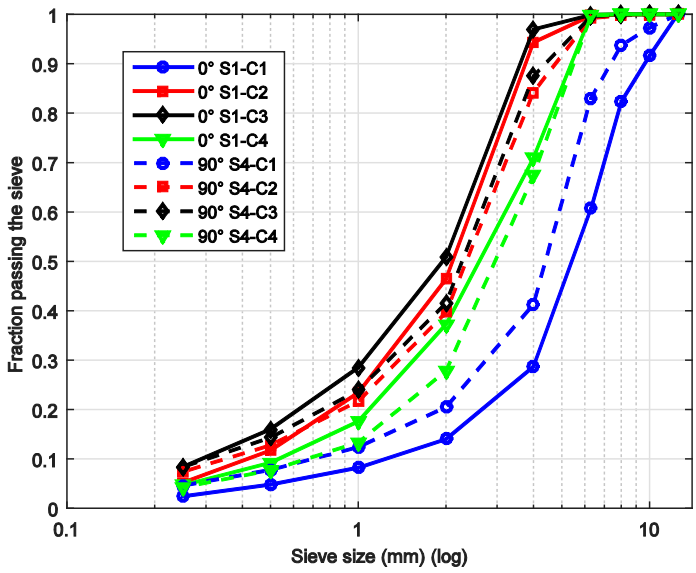

Figure 3: *Product size distribution after the tests with specimen angles of 5° + 5°.*

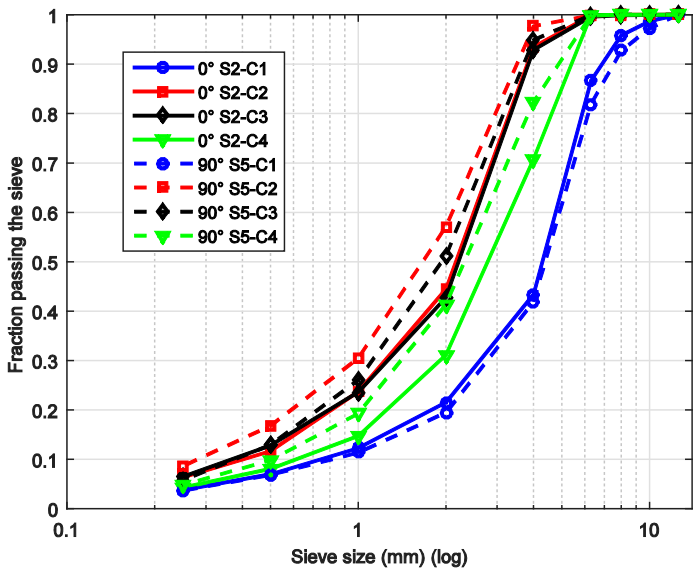

Figure 4: *Product size distribution after the tests with specimen angles of 10° + 0°.*

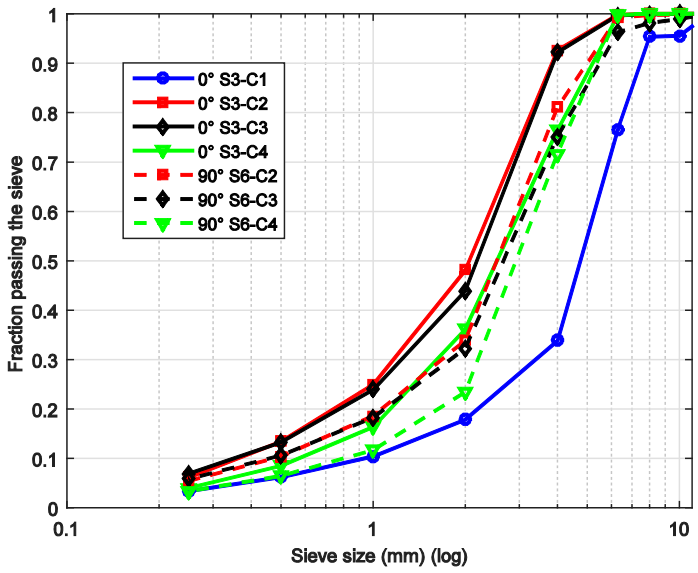

Figure 5: *Product size distribution after the tests with specimen angles of 12.5° + 12.5°.*

The sieved size distribution of the product can be used for rough comparison only. The increase of surface area was therefore estimated from the size distribution to describe the comminution by a single number. The total mass of the particles together with an estimated average mass of the particle in a particular size distribution was used to estimate the number of particles in each sieve range. All particles were assumed to be of average size and spherical, when the surface area of the particles in a sieve range was calculated. Table 3 shows the average rock size and surface area values used in the calculations. The total surface area was calculated as the sum of the surface areas in all sieve ranges for the feed S_F and product S_p. Figure 6 shows the difference $\Delta S = S_P - S_F$ as the increase of the surface area during the tests, where the feed was crushed to the product. The spherical area of the particles is a simple estimation and can cause variations in the results, as the shape of the rock particles can vary with their size. The roughness of the particles is neither taken into account, which could increase the surface area significantly. These factors, however, are assumed to be constant between the different size categories, and even though the actual surface areas of the particles are many times larger, the simplified values can be used in the relative comparison of the tests. Also the finest particles outside the sieve range, which have the largest surface area relative to their mass, are excluded from the estimate. This is partly because they are difficult to measure, and because the finest particles can be

assumed to have only a minor role in the wear of the specimens. Nevertheless, Figure 6 shows that the increased surface area in the tests with C1 and C2 setups was about the same. Also the sum of the increased surface area in the tests with both setups (C1+C2) shows similar size range as the tests with the C3 crushing setup. In this comparison, the average increase of the surface area in the tests with the C1 and C2 setups with reduction ratio of (2:1) was 5.3 $x10^6$ mm^2, while in the tests with the C3 setup with RR of (4:1) it was 9.8 $x10^6$ mm^2. The comparison shows that doubling of the reduction ratio roughly doubles the increase of the surface area of the rock particles in the test.

***Table 3**: Values used to estimate the surface area of the rock particles.*

Sieve range (mm)	Average rock diameter (mm)	Spherical rock weight (g)	Spherical rock surface area (mm^2)
8–10	9	1.0153	254.5
6.3–8	7.15	0.4777	154.9
4–6.3	5.15	0.1740	78.5
2–4	3	0.0376	28.3
1–2	1.5	0.0047	7.07
0.5–1	0.75	0.0005	1.77
0.25–0.5	0.375	$7.34E^{-05}$	0.44
Bottom bin	0.125	$2.72E^{-06}$	0.049

The tests with the C4 setup show generally higher increase of the surface area than the tests with the C1 or C2 setups. The sieved size distribution showed that the C4 setup produces coarser sized rock than the C2 setup, which used the product of the test conducted with the C1 setup as feed. The crushed product of the test with the C1 setup had larger size differences and contained more fine particles than the more homogenous feed of the tests conducted with the C4 setup. When larger particles are crushed, the finer particles can flow through the gape without contacting the jaws. The homogenous feed of the C4 setup required crushing of all particles before they could escape from the gape, which could lead to a higher surface area increase in the tests even when the product size of the test with the C4 setup was larger than in the C1 setup test.

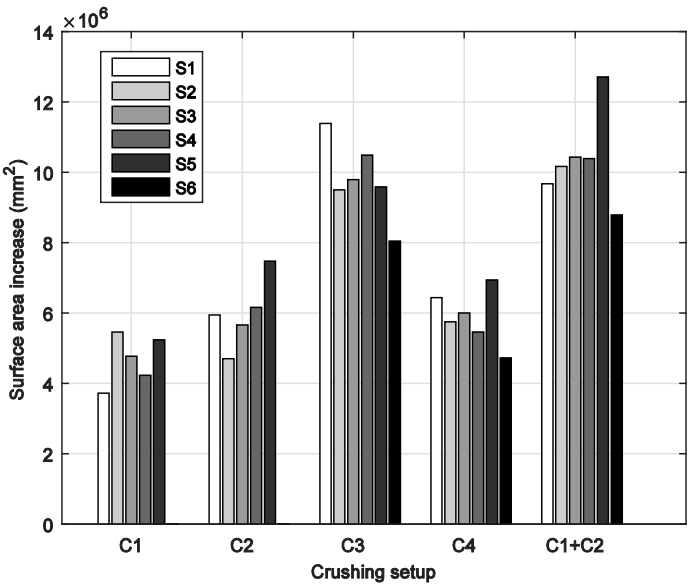

***Figure 6**: Increase of the surface area during crushing.*

3.2 Wear and deformation of specimens

Figure 7a shows the volume wear rate in the tests with the β = 0° setup. The wear in each test is shown with a grey-scaled bar, representing the sum wear rate of both jaw plates, and with white and black bars inside the grey bar to show the wear rates of Jaw1 and Jaw2 specimens separately. Generally, the wear rates of the Jaw1 specimens were slightly higher compared to the Jaw2 specimens. The only major difference between the jaws is in the use of the gape side plates, which in the case of Jaw2 are fixed to specimen holder. In Jaw1,

the side plates move relative to the jaw and therefore there is a slightly larger gap between the sides of the specimen and the side plate, which could introduce some additional wear in the edges of the Jaw 1 specimen, or change the movement of the particles that are supported by the side plates. These differences could be the reason for the higher wear rate of the specimens in Jaw1 in the tests with $\beta = 0°$. The changes in the wear rates with the C2 and C4 setups are relatively similar for all studied jaw angles, but the amount of wear is generally lower with the C4 than with the C2 setup. In the tests with the C1 and C2 setups, the wear rate was higher when finer sized feed is crushed to a finer sized product. The difference in the amount of wear was large when comparing the S1-C1 and S1-C2 tests. The S1-C1 test was repeated to make sure that the low wear rate in the test was correct, but the result was the same. Much higher wear rates were obtained from the S2-C1 test when compared to the S1-C1test. The 10° tilt of the Jaw1 specimen caused higher wear in the Jaw1 compared to the Jaw2 specimen. The uneven wear, however, does not explain why the wear rate is over twice the wear rate of the S1-C1 test. The highest wear rate was obtained with the largest jaw angles for the S3 sample in all C setups. Again, the Jaw1 specimen wear rate was higher than that of the Jaw2 specimen, but in comparison to the tests with the S2 sample, the uneven jaw angles caused a higher wear rate difference between the Jaw1 and Jaw2 specimens. The C3 setup tests with RR = (4:1) can be compared to the sum wear of the tests with the C1 and C2 setups, which result also in the reduction ratio of (4:1). The sum wear rates shown as C1+C2 bars are fairly close to the tests conducted with the C3 setup. The largest difference was observed between the wear rates of tests S2-C3 and S2-(C1+C2), where the sum of the wear rates in the two consecutive tests was higher than in the test with a higher reduction ratio. A similar comparison between S1-C3 and S1-(C1+C2), or between the S3-C3 and S3-(C1+C3), shows much smaller differences in the wear rates, indicating that these tests are less sensitive to whether the crushing is conducted in one or two steps.

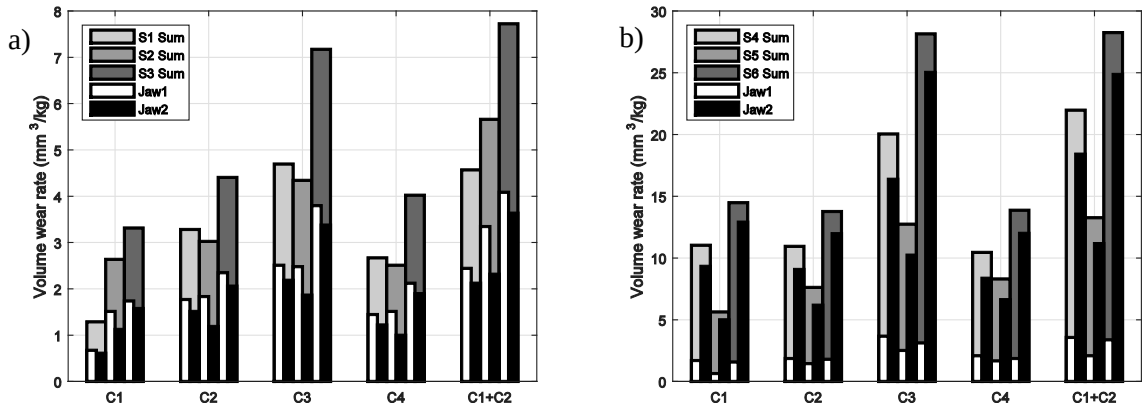

Figure 7: *Wear of Jaw1 (white) and Jaw2 (black) specimens, and the sum wear of both specimens (gray) in the tests with a) $\beta = 0°$ and b) $\beta = 90°$ setups.*

Figure 7b shows the results of the tests with $\beta = 90°$ in a similar manner as for $\beta = 0°$ in Figure 7a. The introduction of lateral movement leads to a significantly higher wear rate of the Jaw2 specimen and much higher overall wear rate compared to the tests done with the $\beta = 0°$ setup. The tests with C2 and C4 setups show similar wear rates, which is also true for the tests with C3 and (C1+C2) setups. The different feed and product sizes in the tests with C1 and C2 setups lead to interesting differences, as wear is more or less similar in the S1 and S3 samples when both specimens have similar jaw angles, whereas the S2-C2 tests show higher wear rates than the S2-C1 tests. However, the tests with the S2 sample show much lower wear rates than with the S1 or S3 samples, where the main difference is the wear rates of the Jaw2 specimen. This difference could be caused by the difference in the speed of the lateral motion between the jaws, when the compressive movement initiates.

The introduction of lateral movement increases the wear rates in the tests by different factors. The wear rate doubles from the S2-C1 and S2-C2 tests to the S5-C1 and S5-C2 tests with the $\beta = 90°$ setup, whereas the wear rates between the S1-C1 and S4-C1 tests increases roughly by a factor of 10. A corresponding factor of 3 in the wear rates was found between the tests S1-C2 and S4-C2. The largest jaw angles of the S3 setup yielded roughly a factor of 4 between the tests with the $\beta = 0°$ and $\beta = 90°$ setups, which otherwise used similar S and C setups. The amount of wear caused by the lateral movement is thus highly dependent on the other test parameters.

The wear rate can also be affected by the different ability of different test configurations to cause work hardening in the manganese steel. In the current study, several tests were conducted with the same specimen pairs, which ruled out the possibility to measure the surface hardness profile after each test. Figure 8 shows the surface hardness (HV 5) profiles measured from both specimens (Jaw1 and Jaw2) of S1 after tests conducted with $\beta = 90°$, and from the Jaw1 specimen of S1 after a test conducted with $\beta = 0°$. Several depth profiles were taken with a 5 mm interval along the 10° taper cross-section prepared on the specimen wear surface. The profiles reveal the rather strong and deep hardening of the Jaw1 specimens, while the hardening of the Jaw2 specimens is shallower and less extensive. The lateral movement of the jaws slides the rock particles against the Jaw2 wear surface, causing a faster rate of material removal and decreasing the net effect of hardening, which could be one reason for the lower hardness values. Another possibility for the lower hardness is that the deformation mechanism of the manganese steel somehow changes with the introduction of the sliding particles.

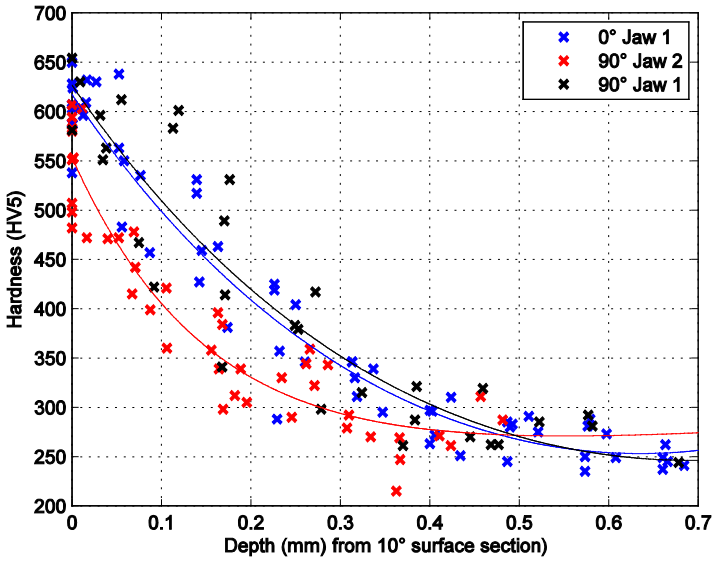

Figure 8: *Hardness profiles of the Jaw1 specimen from the S1-C1 test (blue) and the Jaw1 (black) and Jaw2 (red) specimens from the S4-C1 test.*

3.3 Energy consumption

Figure 9a shows the work done in the DPJC tests with the $\beta = 0°$ setup. The white and black bars in Figure 9a show the work done in the Z and Y directions, whereas in Figure 9c the work is shown in directions Z_2 and Y_2 that are aligned normal and perpendicular to the Jaw2 specimen wear surface. Work was accumulated mostly in the Z direction, which is the compressive direction of the jaw crusher. In the tests with the S3 setup, small amount of work is also done in the Y_2-direction because of the larger jaw angles of the specimens. The amount of work follows the trend of the specimen wear rates shown in Figure 7, the largest amount of work being consumed in the tests with the largest jaw angles. The amount of work is also more or less the same in the test with the C3 setup and in the C1 and C2 tests combined.

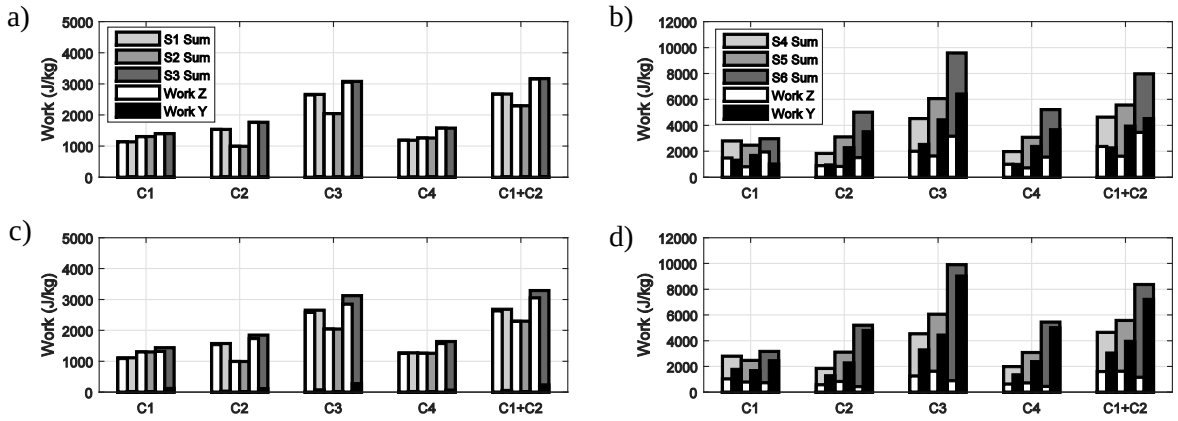

Figure 9: *The consumed work a) and b) in Z (white) and Y (black) directions, and c) and d) in Z_2 and Y_2 directions, and the sum of the work (grey) from the tests with a) and c) the $\beta = 0°$, b) and d) the $\beta = 90°$ setup.*

Figure 9b presents the consumed energy in the tests with the β = 90° setup. The tests with the C2 and C4 setups yield quite similar results, as does the C3 test with the combination test C1+ C2. The test S3-C3 shows higher energy consumption than the sum of the tests S3-C1+C2. The increase in the amount work takes place mainly in the Y-direction. In contrast to the wear rates observed in the tests, the energy consumption is higher with the S2 setup than with the S1 setup. The only exception is the S1-C1 test, where the amount of work done is slightly higher than in the S2-C1 test.

3.4 Force and friction in the test

Figure 10 shows how much work is done at different contact force levels in different tests. For example, Figure 10a shows that with the C1 setup most of the work is done with contacts of ca. 2 kN, and that the contact forces are slightly higher in the tests with β = 0° than with β = 90°. Setup C2 with smaller feed size in Figure 10b shows smaller contact forces compared to setup C1. Also the shapes of the histograms are different. Setup C3 in Figure 10c shows features of both C1 and C2: the contact forces are higher and their distribution is wider, which could be caused by the larger number of supporting contacts between the jaws and the rock particles. The larger rocks are located higher between the jaws than the smaller rocks, and therefore both of them can become compressed at the same time. As seen in Figure 10d, the lowest contact forces are measured in the tests with the C4 setup, where the rocks are small and their size distribution is narrow.

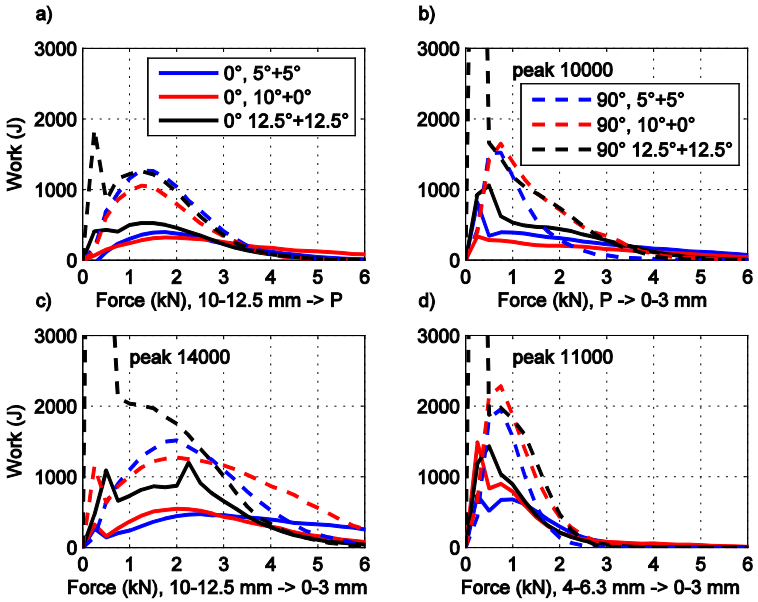

Figure 10: *Work accumulated at different contact forces in the tests with a) C1, b) C2, c) C3 and d) C4 crushing setups. The solid lines present the β = 0° setup and the dashed lines the β = 90° setup.*

The jaw angles seem to have a minor effect on the resultant contact force, but they appear to cause quite much variation in the coefficient of friction in the tests. Figure 11a shows the amount of work as a function of the coefficient of friction in the tests with the C1 setup. The coefficient of friction is similar in the tests with the β = 90° setup, but is affected more by the jaw angles in the tests with the β = 0° setup. Other crushing setups with smaller rocks sizes in Figure 11b and d show similar behavior, having the peaks of the coefficient of friction histograms at the same positions. The highest values of the coefficient of friction were measured with the largest jaw angles, and the lowest with the 10°+0° setup. There does not seem to be much difference in the coefficients of friction between the tests with 5°+5° and 10°+0° jaw angles and β = 90°. The coefficient of friction of the C3 setup in Figure 11c seems to be a mixture of the C1 and C2 setups. For example, the test with 12.5° +12.5° jaw angles and the β = 90° setup seems to have the peak in the coefficient of friction values between the peak values of the C1 and C2 tests.

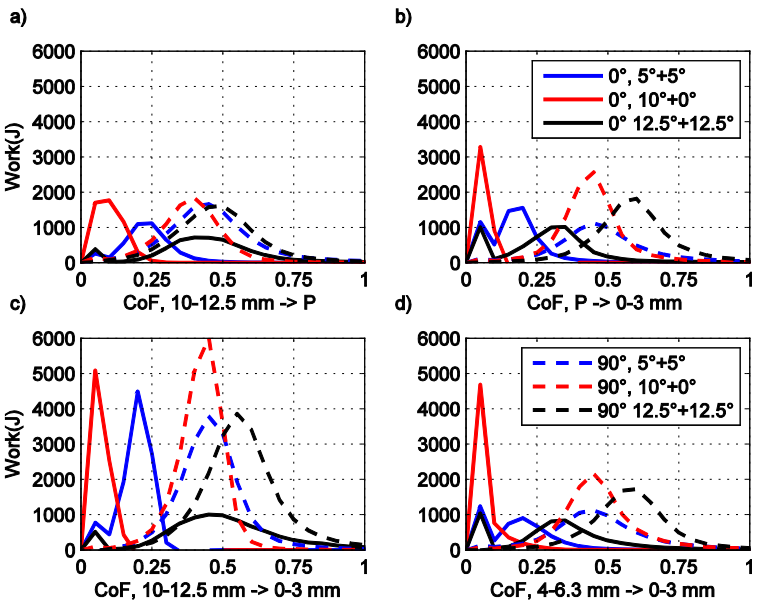

Figure 11: *Work accumulated at different coefficients of friction in the tests with a) C1, b) C2, c) C3 and d) C4 crushing setups. The solid lines present the β = 0° setup and the dashes lines the β = 90° setup.*

4. DISCUSSION

The presented results describe the behavior of the DPJC test system when the test parameters are changed. To identify the differences between the different test setups, it is important to compare all the three main outcomes of the tests. The crushing product size was found to depend mainly on the open and closed site settings, but to be also affected by the size distribution of the feed. The size reduction, or the increase in the total particle surface area, can be used in the comparison of the other test outcomes. The increase in the reduction ratio from (2:1) to (4:1) roughly doubles also the wear rate and the work done in the tests. Test S1-C1 shows the lowest increase in the rock surface area, wear rate, and accumulated work. The other tests, S2-C1 and S3-C1, follow this same trend with slightly higher values of wear, work, and increase of the surface area. The change in the lateral movement between the tests with $\beta = 0°$ and $\beta = 90°$ does not markedly change the size of the product, but the amount of both the wear and work increase significantly. This indicates that even though the energy consumption and the capacity of the crusher changes, the actual crushing of the rock is very similar. The lateral movement of the jaws can slide the rocks against the specimen plates and thus contribute to the generation of fines, but this behavior cannot be confirmed by these tests. As shown in Figures 10 and 11, the lateral movement affects the loading direction, which could lead to differences in the crushing of elongated particles. The shape of the jaw crusher may cause elongated rocks to align their longer axis parallel to the vertical direction of the jaw. If the mineral has a tendency to fracture along certain planes that intersect at a 90° angle, the elongated orientation could turn the mineral so that one of its planes becomes aligned close to the compressive direction. Some granites are reported to show anisotrophic mechanical properties [15], and therefore a change in the compression direction due to the lateral movement of the rock could cause changes in its crushability. A spherically shaped rock will align more randomly, which could lead to a different crushability compared to the elongated rocks. The sieve method with square shaped meshes does not separate particles according to their most elongated direction, but rather by the direction where the rock has the smallest dimensions. In the present study, granite from the same rock batch was used, and therefore the shape of the rock particles within one sieve category should be the same in all tests.

4.1 Relation between wear and work

The amount of wear in the DPJC specimen plates is increased with increasing lateral movement of the jaws, most of the increase concentrating on the Jaw2 specimens. The lateral movement increases also the amount of work done in the test, again primarily in the lateral Y-direction. Most of this work can be assumed to originate from the contacts that produce wear in the specimen plates, as the comminution of the particles is fairly constant in the tests with different β setups. Figures 12a and 13a show the relations between the volumetric wear rate and work, when the tests are done with different β setups but similar crushing and jaw angle setups, as for example in tests S1-C1 and S4-C1. As the other parameters are similar, the increase in wear and work can be assumed to be due to the increase of the lateral movement. The fitted lines seem to cross the x-axis at around 1000 J, when the reduction ratio of the test is close to (2:1), and at around 2000 J, when the reduction ratio is close to (4:1). These values can be interpreted as minimum amounts of work required to crush one kilogram of granite in the test. There are, however, some variations in the results, especially in the tests with samples S2 and S5, where the x-axis crossing point is at a much lower value. This means that the wear rate and work are not directly related but also some other parameters affect the outcome. Archard's [16] equation can be used to assess the relation between wear and work:

$$\frac{W_V}{L} = K\frac{F_N}{H} \qquad (1)$$

where W_V is the volumetric wear rate, L is the sliding distance, K is the wear related constant, F_N is the normal force, and H is the hardness of the surface where sliding occurs. As work is the product of the tangential force F_t over the sliding distance, i.e., $W_{work}=F_t L$, we can write:

$$F_N = \frac{F_t}{\mu} = \frac{W_{work}}{\mu L} \qquad (2)$$

where μ is the coefficient of friction. Substituting Equation 2 into the Archard's Equation 1 we obtain:

$$\frac{W_V}{L} = K\frac{F_N}{H} = K\frac{W_{work}}{\mu HL} \quad (3$$

which can be written as:

$$\frac{W_V}{W_{work}} = K\frac{1}{\mu H_{def}} \quad (4)$$

where H_{deff} is the deformed hardness of the wear surface. Figure 12b and13b show the correlation between wear and work, when the wear rate of the specimens is multiplied by the measured coefficient of friction in the test and the hardness of the wear surfaces. The coefficient of friction is obtained from the peaks in Figure 11, where the accumulated work is highest. The wear coefficient K should be constant regardless of the amount of sliding movement in the test, and it is determined as the slope of the line between the test pairs with β = 0° and β = 90° setups.

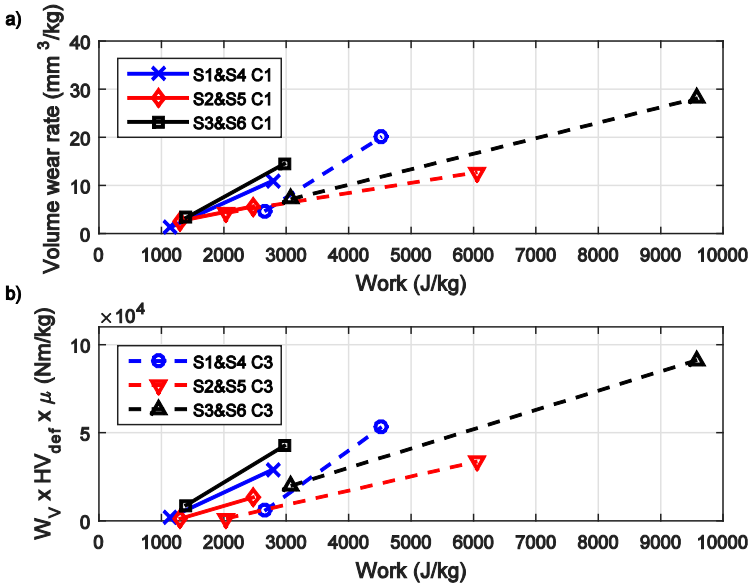

Figure 12: *Relation between a) wear and work in the tests with C1 and C3 crushing setups, and b) relation between work and wear modified by the average friction coefficient and hardness. Tests with the same specimen angles are paired to show the development of wear and work as the lateral movement of the jaws is changed.*

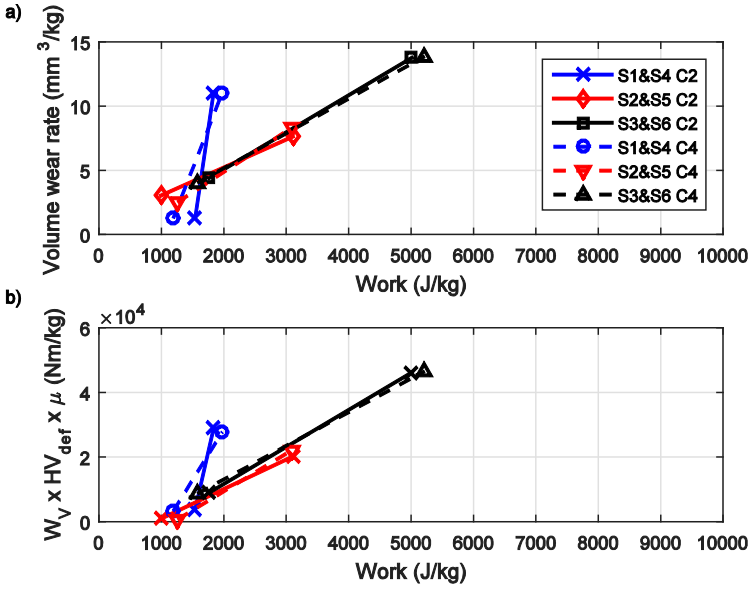

Figure 13: *Relation between a) wear and work in the tests with C2 and C4 crushing setups, and b) relation between work and wear modified by the average friction coefficient and hardness. Tests with the same specimen angles are paired to show the development of wear and work as the lateral movement of the jaws is changed.*

Figure 13b shows a comparison of the tests with C2 and C4 setups. The sample pair S1&S4 has the steepest slope in the plot, which indicates that wear requires less energy in these tests. All tests with sample pairs S2&S5 and S3&S6 have the same slope in the work-wear linear fits, which means that the amount of work needed to wear the specimen is more or less the same. The difference between the tests is that more work was consumed in the tests with the S3&S6 than with the S2&S5 samples, and that also the specimen wear was higher with the S3&S6 samples. This could have been caused by the increased amount of slipping of rock particles in the wider gape, which increases work and wear, but the mechanism of wear was essentially similar in the tests with S3&S6 and S2&S5 sample pairs.

Figure 14 shows a comparison of the same tests as in Figure 12, where the amounts of wear with C1 and C2 setups are accumulated, showing an increase of wear and work in both tests with the same β value. The endpoints of the accumulated lines are comparable to the test with the C3 setup. The comparison shows that all results from the tests with β = 0° and from the tests with S2 and S5 setups and β = 90° have a similar slope, whereas the slopes from the tests with the S4 and S6 setups is steeper. Figure 14 also shows that the reason for the steeper slope of the S1&S4 C3 test pair compared to the other C3 pairs can be explained with the steeper slopes of the S4 C1+C2 test pair.

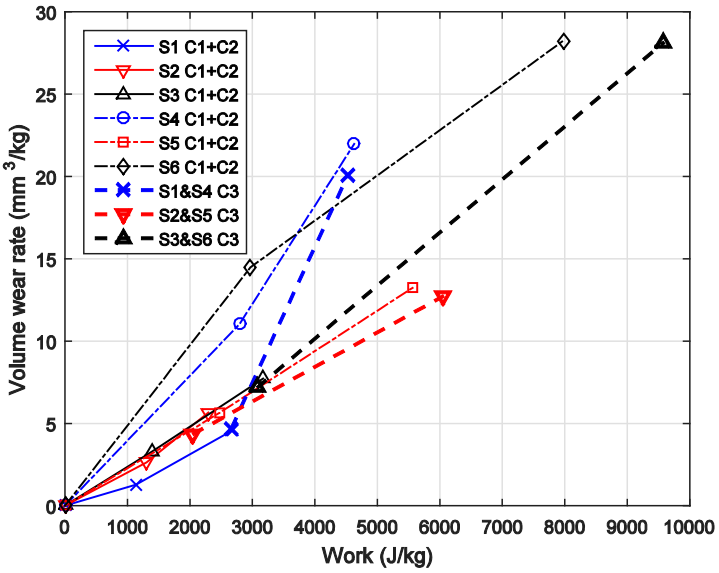

***Figure 14**:Relation of wear and consumed work of the tests with the C1 C2 and C3 setups, where the C1+C2 shows the cumulating wear and work of the tests added sequentially. The tests with the C3 setup show fairly similar results with the cumulated C1+C2 end points.*

The different results in the tests with S4 samples could be explained by the higher velocity between the jaws at the beginning of the crushing cycle, accompanied by low enough jaw angles to prevent excessive slipping of the rock particles. Larger jaw angles could cause a situation where high contact forces cause only short and shallow sliding before slipping and losing contact with both jaws. Figure **15** shows a comparison between the Jaw2 specimens in tests S4-C1 and S6-C1. The stereo microscope images are taken from the same location in each specimen, where the center of the image is roughly 30 mm from the lower end of the specimen. The lower end is towards the bottom of the images, and the sliding direction of the particle on the specimens is from the lower end to the top end. The S4-C1 test in Figure 15a clearly shows deeper penetrations of the particles. The microscopic investigation also showed cutting chips still in contact with the wear surface of the S4-C1 Jaw2 specimen. These chips had a yellowish color similar to the tempering colors of steels, indicating that the chip temperature rising high enough to build an oxide layer on the surface. Similarly colored features were not found from the other specimens.

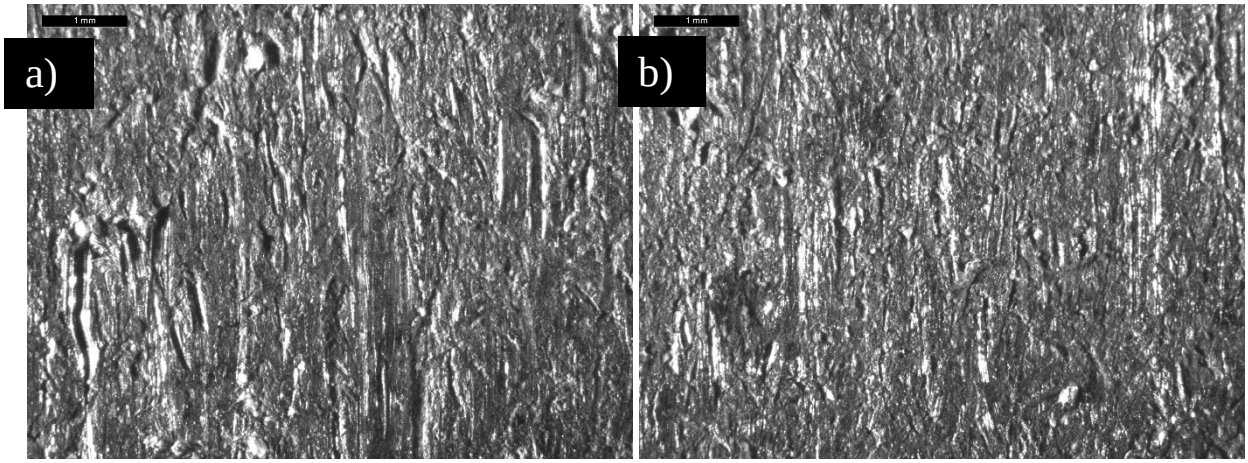

***Figure 15:** Wear surface of Jaw2 specimen from a) S4-C1 and b) S6-C1 test, taken approximately from the same relative location.*

5. CONCLUSIONS

- The wear rate of the manganese steel in the DPJC test is highly dependent on the test configuration. The test matrix shows that increase in the jaw angles and the lateral movement between the jaws, and thus sliding, causes increased wear even though the comminution of the rock can be similar in the tests.
- The consumed energy (or work done) usually follows the trend of wear, and the results show that they are closely related. The energy can be assumed to be spent in two different types of events: crushing of the rock, and sliding and wear contacts of the specimens with the rock particles. These energy components can also be independent and not affecting each other.
- The comminution of the rock in the tests is mostly dependent on the release end settings, which determine the size range of the gap that the particles need to pass thought to exit the crusher. Until that point the particles remain in the system and increase both wear of the specimens and the consumed energy. The size distribution of the feed has also a minor effect on the comminution, wear and work in the test.
- The wear and work results obtained from the tests with different lateral movement of the jaws allow to determine the wear coefficient K for each test configuration. The higher initial crushing speed decreases the amount of work needed to remove material from the specimen surface, i.e. to cause wear, in a DPJC crushing test.

6. ACKNOWLEDGEMENTS

The work has been done within the FIMECC DEMAPP (2009-2014) and FIMECC BSA programs funded by Tekes and the participating companies.

7. REFERENCES

1. T. Napier-Mun. Is progress in energy-efficient comminution doomed? Minerals Engineering, 73, 1–6, 2015.
2. R.T. Hukki. Proposal for a solomonic settlement between the theories of Von Rittinger, Kick and Bond. Transactions on AIME, 220:403–408, 1961.
3. D.W Fuerstenau and A.-Z.M Abouzeid. The energy efficiency of ball milling in comminution, International Journal of Mineral Processing, 67, 1–4, 161–185, 2002.
4. Desmond Tromans. Mineral comminution: Energy efficiency considerations. Minerals Engineering, 21(8): 613–620, 2008.
5. J. De la Vergne. Hard Rock Miners's Handbook. Stantec Consulting Ltd., 5th edition, 2008.
6. A. Tosun and G. Konak. Development of a model estimating energy consumption values of primary and secondary crushers. Arabian Journal of Geosciences, pages 1–12, 2014.
7. L. Workman and J. Eloranta. The effects of blasting on crushing and grinding efficiency and energy consumption. Proceedings of the Annual Conference on Explosives and Blasting Technique, 1, 131-140, 2003.
8. K. Schoenert. SME Transactions, 252, 21–26, 1972.
9. B.W.E. Avient, J. Goddard, and H. Wilman. An experimental study of friction and wear during abrasion of metals. Proc. R. Soc. Lond. A., 258(1293):159–180, 1960.
10. J. Goddard and H. Wilman. A theory of friction and wear during the abrasion of metals. Wear, 5(2):114–135, 1962.
11. ASTM G81-97a, Standard practice for jaw crusher gouging abrasion test. ASTM International, West Conshohocken, PA, 2013.
12. Korman T., Bedekovic G., Kujundzic T., Kuhinek D. Impact of physical and mechanical properties of rocks on energy consumption of jaw crusher, Physicochem. Probl. Miner. Process. 51(2), 461−475, 2015.
13. M. Lindqvist and C.M. Evertsson. Linear wear in jaw crushers. Minerals Engineering, 16(1):1–12, 2003.
14. J. Hautalahti. Laboratoriomenetelmät kiven murskattavuuden arvioimiseksi. Tampere University of Technology, M.Sc. Thesis 1996.

15. Y. Nara. Effect of Anisotropy on the Long-Term Strength of Granite, Rock Mech Rock Eng, 48, 959–969, 2015.
16. J.F. Archard. Contact and rubbing of flat surfaces. Journal of Applied Physics, 24(8):981–988, 1953.